A Photometric Study of the Eclipsing Binary Star V2790 Orionis

Edward J. Michaels
Stephen F. Austin State University, Department of Physics and Astronomy, P.O. Box 13044, Nacogdoches, TX 75962; emichaels@sfasu.edu

Received February 2, 2016; revised May 26, 2016, Accepted May 31, 2016

Abstract Presented in this paper is the first precision set of multi-band light curves for the eclipsing binary star V2790 Ori. A new linear ephemeris gives an orbital period of 0.28784176 d. The light curves were analyzed with the Wilson-Devinney program to determine the best-fit stellar model. Star spots were required in the model to account for asymmetries in the light curves. The synthetic light curve solutions presented are consistent with a W-type contact binary.

1. Introduction

V2790 Ori (TYC 1322-294-1, GSC 01322-00294) was identified as an eclipsing binary by Otero *et al.* (2004) from the public data release of the Northern Sky Variability Survey (NSVS; Wozniak *et al.* 2004). The star was classified as an EW type with a period of P = 0.287842 d. Also using observations from the NSVS database, Gettel *et al.* (2006) found that the V-band magnitude ranged from V_{max} = 11.181 to V_{min} = 11.743, and using a newly derived period-color relation estimated a distance of 199 pc. Only a few times of minima have been reported for this system. In this paper a photometric study of V2790 Ori is presented. It is organized into sections with observations and data reduction techniques presented in section 2, period analysis and Wilson-Devinney (WD) models in section 3, and discussion and conclusions in section 4.

2. Observations

Photometric observations of V2790 Ori were acquired using the 0.31-m Ritchey-Chrétien robotic telescope at the Waffelow Creek Observatory (http://obs.ejmj.net/index.php). An SBIG-STXL camera with a KAF-6303E CCD (9μm pixels) was used for imaging on several nights in 2015. Observations using Sloan g', r', and i' passbands were made on January 7, 17, 18, 19, 23, 26, 27. These observations comprise Data Set 1 (DS1). Additional observations were made in the Johnson B and V passbands on November 18 and 19 which comprise Data Set 2 (DS2). A total of 4,651 images were acquired: 449 in Johnson B, 447 in Johnson V, 1,102 in Sloan g', 1,443 in Sloan r', and 1,210 in Sloan i'. Only one passband was observed on each of the January dates to improve cadence while on the November dates both Johnson B and V observations were acquired. All images were calibrated with bias, dark, and flat field frames. MIRA software (Mirametrics 2015) was used for calibration and ensemble differential aperture photometry.

Listed in Table 1 are the coordinates and standard magnitudes of the five comparison stars and the check star (K) used in this study. The standard magnitudes for each passband were taken from the AAVSO Photometric All-Sky Survey (APASS; Henden *et al.* 2014). The instrumental magnitudes for V2790 Ori were converted to standard magnitudes using these comparison stars. A finder chart for these stars is shown in Figure 1. The folded light curves for each passband in standard magnitudes are shown in Figure 2. The time of each observation (T) was converted to orbital phase Φ using

$$\Phi = \frac{T - T_0}{P} - \text{Int}\left(\frac{T - T_0}{P}\right) \quad (1)$$

where T_0 is a time of minimum for a primary eclipse (epoch) and P is the orbital period. Throughout this paper the values used for epoch and period are T_0 = 2357346.7442 and P = 0.28784176 day (see section 3.1). All light curve figures are plotted from phase –0.6 to 0.6 with negative orbital phase defined as Φ – 1. Also shown in the bottom panel of Figure 2 are all the standard Johnson V-magnitudes for the K star. The K star magnitudes listed in Table 1 are averages from all observations for each passband. These average values compare well with the APASS all-sky photometry. For each night a plot of the K star magnitudes was inspected and no significant variability was detected. All the observations in this study are available from the AAVSO International Database (Kafka 2015).

3. Analysis

3.1. Period determination

Using the Kwee and van Woerden (1956) method 14 new times of minima were determined from both DS1 and DS2 observations. These new minima times and all others found in the literature are reported in Table 2. The initial ephemeris used in this study was taken from Otero (2004) and is given by:

$$\text{HJD Min I} = 2451521.695 + 0.287842\ E. \quad (2)$$

Using all the available times of minima an improved ephemeris was determined by least-squares solution and is given by:

$$\text{HJD Min I} = 2457346.7442\ (3) + 0.28784176\ (9)\ E. \quad (3)$$

Figure 3 shows the O–C diagram from Equation 3. There appears to be no secular period change but the O–C diagram hints at a possible small cyclic change. This type of period change could possibly be caused by a third body in the system. A third body in a contact binary is not uncommon but the minima times presently available cannot yet support this supposition since the observations only span about 5 years. Several years of additional times of minima will be necessary to verify if a period change is actually occurring and its cause.

Table 1. Variable (V), comparison (C), and check (K) stars in this study.

Star	*R.A. (2000)* *h m s*	*Dec. (2000)* ° ′ ″	*B*	*V*	*g′*	*r′*	*i′*	*(B–V)*
V2790 Ori (V)	06 15 31.4	+19 35 22.0						
GSC1322-0961 (C1)	06 15 06.6	+19 32 05.5	11.425	11.002	11.180	10.938	10.913	0.423
			± 0.029	± 0.022	± 0.055	± 0.017	± 0.026	± 0.036
GSC1322-1399 (C2)	06 15 19.7	+19 37 06.6	11.379	11.052	11.181	11.022	11.050	0.327
			± 0.032	± 0.030	± 0.067	± 0.023	± 0.036	± 0.044
GSC1322-1132 (C3)	06 15 35.9	+19 37 58.9	12.420	11.781	12.082	11.607	11.456	0.639
			± 0.034	± 0.024	± 0.070	± 0.023	± 0.037	± 0.042
GSC1322-0698 (C4)	06 15 03.6	+19 33 05.1	12.327	11.825	12.048	11.714	11.642	0.502
			± 0.026	± 0.027	± 0.059	± 0.011	± 0.012	± 0.037
GSC1322-0494 (C5)	06 15 39.4	+19 35 36.6	13.284	12.128	12.686	11.714	11.299	1.156
			± 0.037	± 0.032	± 0.106	± 0.038	± 0.067	± 0.049
GSC1322-1333 (K)	06 15 42.0	+19 38 27.5	11.671	10.769	11.180	10.451	10.219	0.902
			± 0.030	± 0.067	± 0.082	± 0.025	± 0.038	± 0.073
Observed check star magnitudes (K)			11.688	10.733	11.148	10.427	10.231	0.935
			± 0.007	± 0.005	± 0.008	± 0.009	± 0.008	± 0.009

APASS comparison and check star magnitudes and errors. The observed check star magnitudes are the averages over all nights for each passband.

Table 2. Available times of minima and O–C residuals from Equation 2.

Epoch HJD 2400000+	*Error*	*Cycle*	*O-C Linear*	*References*
55520.82050	0.00020	–387.5	0.0005	Nelson 2011
55532.91030	0.00040	–345.5	0.0009	Diethelm 2011
55604.29500	0.00040	–97.5	0.0009	Nagai 2012
55632.35970	0.00040	0.0	0.0010	Nagai 2012
55644.30500	0.00040	41.5	0.0008	Nagai 2012
55896.88270	0.00030	919.0	–0.0026	Diethelm 2012
55902.78500	0.00010	939.5	–0.0010	Nelson 2012
55959.34660	0.00020	1136.0	–0.0004	Hübscher 2013
56288.06100	0.00040	2278.0	–0.0012	Nagai 2013a
56288.20450	0.00040	2278.5	–0.0017	Nagai 2013a
56623.10920	0.00040	3442.0	–0.0008	Nagai 2013b
56623.25470	0.00040	3442.5	0.0007	Nagai 2013b
57041.63261	0.00007	4896.0	0.0007	Present observations
57041.77672	0.00005	4896.5	0.0008	Present observations
57042.64031	0.00005	4899.5	0.0009	Present observations
57042.78361	0.00006	4900.0	0.0003	Present observations
57048.68477	0.00013	4920.5	0.0007	Present observations
57048.82855	0.00007	4921.0	0.0005	Present observations
57049.69193	0.00007	4924.0	0.0004	Present observations
57049.83623	0.00007	4924.5	0.0008	Present observations
57050.69948	0.00006	4927.5	0.0005	Present observations
57050.84323	0.00008	4928.0	0.0003	Present observations
57345.73605	0.00019	5952.5	–0.0007	Present observations
57345.87983	0.00017	5953.0	–0.0009	Present observations
57346.74338	0.00016	5956.0	–0.0008	Present observations
57346.88755	0.00013	5956.5	–0.0006	Present observations

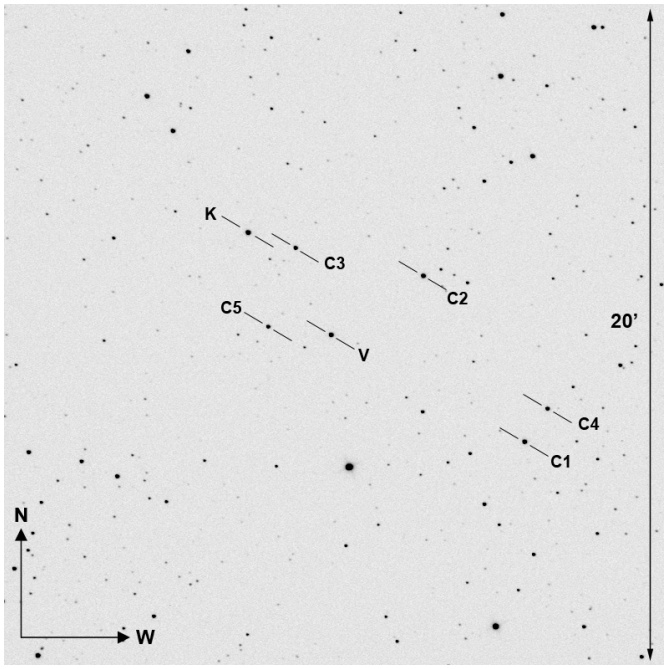

Figure 1. Finder chart for V2790 Ori (V), comparison (C1, C2, C3, C4, and C5) and check (K) stars.

3.2. Temperature, spectral type

V2790 Ori has not been observed spectroscopically, therefore it was necessary to estimate the effective temperature and spectral type from the observed color index. The B and V observations of DS2 were binned with a phase width of 0.01. Both phase and magnitude were averaged in each binned interval. The binned V-magnitudes were then subtracted from the linearly interpolated binned B-magnitudes to form the color index values. These values were averaged at quadrature from phase 0.0 to 0.5. ($\Phi = \pm 0.25$). The resulting observed color index is (B–V) = 0.723 ± 0.010. Figure 4 shows the binned V-magnitude light curve, with the color index shown in the bottom panel. The observed color index of the larger cooler primary star can be determined at phase 0.0, which is a total eclipse. The color index at primary eclipse ($\Phi = \pm 0.05$) has a value of (B–V) = 0.742 ± 0.012. The map of interstellar medium (ISM) dust by Schlafly *et al.* (2014) was not used to determine the color excess for this star. The ISM dust tends to be rather clumpy in this region of the sky due to the star's proximity to the galactic equator (galactic latitude of +1.26°). To determine the effect of dust on this star requires an independent estimate of the color. One method for estimating the star's color index is to use Wang's (1994) period-color relationship for contact binaries given by:

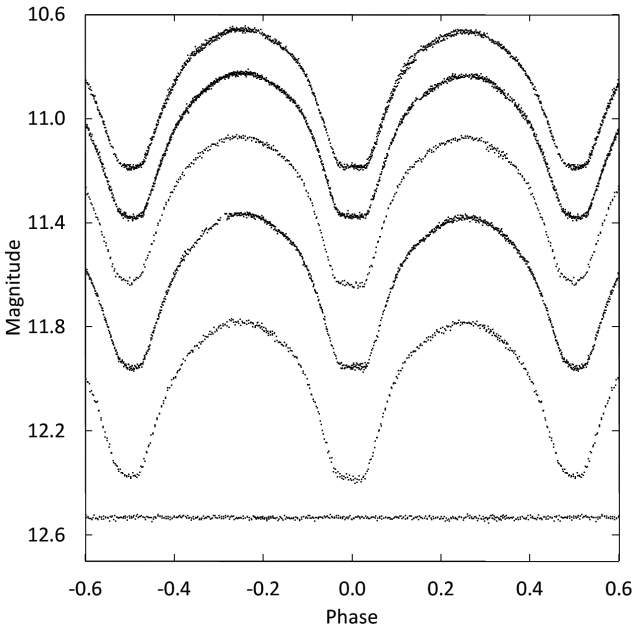

Figure 2. Folded light curves for each observed passband. The differential magnitudes of the variable were converted to standard magnitudes using the calibrated magnitudes of the comparison stars. From top to bottom the light curve passbands are Sloan i', Sloan r', Johnson V, Sloan g', and Johnson B. The bottom curve shows the standard Johnson V magnitudes of the check star (offset +1.8 magnitudes). The standard deviations of check star magnitudes (all nights) are shown in Table 1. Error bars are not shown for clarity.

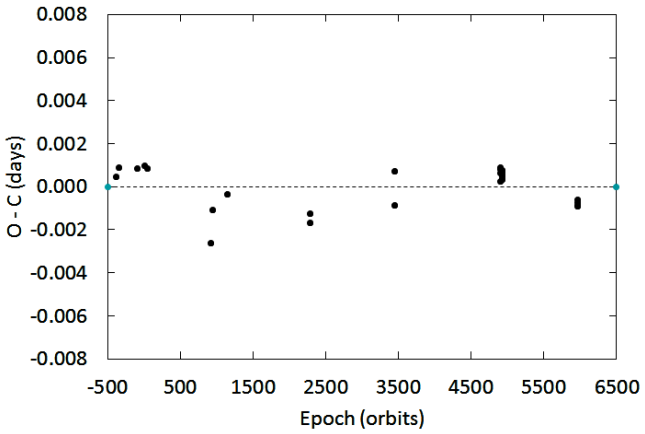

Figure 3. O–C residuals from linear ephemeris fit of Equation 2.

$$(B–V)_0 = 0.62 – 1.31 \log_{10} P. \quad (4)$$

Using the orbital period determined in section 3.1 gives a value of $(B–V)_0 = 0.771$. A second method for estimating the color index is to use Qian's (2003) mass-period relation given by:

$$M = 0.391 (\pm 0.059) + 1.96 (\pm 0.17) P. \quad (5)$$

The calculated value for the more massive star is $M_2 = 0.96 \pm 0.07 M_\odot$. Using Table 5 of Pecaut and Mamajek (2013) gives a color index of $(B – V)_0 = 0.719$ for a main-sequence star of this mass. Both of these estimates indicate dust reddening is not significant for this star. The observed color index at primary eclipse should therefore give a reasonable estimate for the

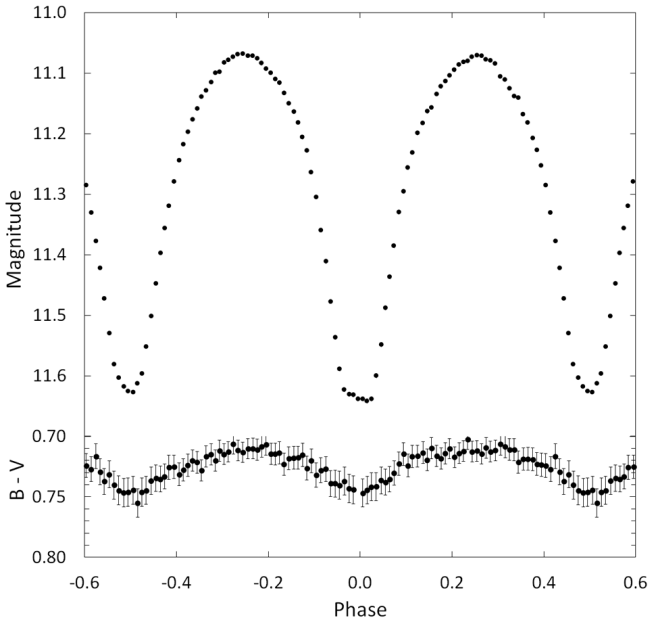

Figure 4. Light curve of all V-band observations in standard magnitudes (top panel). The observations were binned with a phase width of 0.01. The errors for each binned point are about the size of the plotted points. The B–V colors (bottom panel) were calculated by subtracting the binned V magnitudes from the linearly interpolated binned B magnitudes.

effective temperature. Table 5 of Pecan and Mamajek (2013) gives an effective temperature of 5471K and a spectral type of G8 for the larger cooler star.

3.3. Synthetic light curve modeling

For light curve analysis BINARY MAKER 3.0 (BM3; Bradstreet and Steelman 2002) and the Wilson-Devinney program (WD; Wilson and Devinney 1971; Wilson 1990; Van Hamme and Wilson 1998) were used. There were 8 months separating the observations of DS1 and DS2. It was therefore decided to perform independent solutions for each data set. The solutions could then be compared for consistency and for changes in spot configurations, if any. The observations of DS1, passbands g', r', and i', were used for Solution 1 (S1) and DS2 observations, passbands B and V, were used for Solution 2 (S2). The observations in each passband were binned with a phase interval of 0.01. The average number of observations in each bin was 12 for the Sloan g', r', and i' passbands and 5 for Johnson B and V. The binned magnitudes were converted to relative flux for modeling. BM3 was used first to fit a synthetic light curve to the Sloan g' observations. Standard convective parameters and limb darkening coefficients from Van Hamme's (1993) tabular values were used. The total eclipses provided the necessary constraints for finding the mass ratio. The values from this initial fit were used as the input parameters for computation of a simultaneous 3-color light curve solution for S1 and a 2-color solution for S2 using the WD program. The weight attached to each binned data point for the WD solution was equal to the number of observations forming that point. The light curves indicate a likely contact configuration; therefore, Mode 3 was set in the program. The Method of Multiple Subsets (MMS) (Wilson and Biermann 1976) was employed to minimize

Table 3. V2790 Ori synthetic light curve solutions.

Parameter (no spots)	*Symbol (with spots)*	*Solution 1 (S1) (no spots)*	*Solution 1 (S1) (with spots)*	*Solution 2 (S2) (no spots)*	*Solution 2 (S2) (with spots)*
Gravity Darkening	$g_1 = g_2$	0.32	0.32	0.32	0.32
Bolometric Albedo	$A_1 = A_2$	0.50	0.50	0.50	0.50
Inclination	(°)	83.98 ± 0.26	84.15 ± 0.20	83.79 ± 0.25	83.43 ± 0.21
Effective Temp.	T_1, T_2 (K)	5620 ± 4, 5471	5620 ± 3, 5471	5624 ± 4, 5471	5625 ± 4, 5471
Surface Potential	$\Omega_1 = \Omega_2$	6.730 ± 0.014	6.732 ± 0.010	6.731 ± 0.018	6.731 ± 0.018
Mass Ratio	$q(M_2 / M_1)$	3.168 ± 0.012	3.157 ± 0.008	3.140 ± 0.017	3.141 ± 0.017
Fill-Outs	$f_1 = f_2$	0.17	0.15	0.12	0.12
Luminosity	$L_1 / (L_1 + L2)_{g'}$	0.2966 ± 0.0007	0.2966 ± 0.0007	—	—
	$L_1 / (L_1 + L2)_{r'}$	0.2867 ± 0.0005	0.2867 ± 0.0005	—	—
	$L_1 / (L_1 + L2)_{i'}$	0.2830 ± 0.0005	0.2830 ± 0.0005	—	—
	$L_1 / (L_1 + L2)_B$	—	—	0.3021 ± 0.0007	0.3024 ± 0.0007
	$L_1 / (L_1 + L2)_V$	—	—	0.2919 ± 0.0006	0.2921 ± 0.0006
Limb Darkening	$x_{1g'}$, $x_{2g'}$	0.838, 0.840	0.838, 0.840	—	—
	$y_{1g'}$, $y_{2g'}$	0.091, 0.064	0.091, 0.064	—	—
	$x_{1r'}$, $x_{2r'}$	0.760, 0.767	0.760, 0.767	—	—
	$y_{1r'}$, $y_{2r'}$	0.214, 0.194	0.214, 0.194	—	—
	$x_{1i'}$, $x_{2i'}$	0.680, 0.686	0.680, 0.686	—	—
	$y_{1i'}$, $y_{2i'}$	0.238, 0.221	0.238, 0.221	—	—
	x_{1B}, x_{2B}	—	—	0.853, 0.853	0.853, 0.853
	y_{1B}, y_{2B}	—	—	0.039, 0.009	0.039, 0.009
	x_{1V}, x_{2V}	—	—	0.797, 0.802	0.797, 0.802
	y_{1V}, y_{2V}	—	—	0.165, 0.142	0.165, 0.142
Residuals	$\sum res^2$	0.0196	0.0056	0.0082	0.0053
Spot 1 on Star 1			Hot Spot		Hot Spot
Colatitude	(°)	—	105 ± 5	—	100 ± 8
Longitude	(°)	—	10 ± 3	—	7 ± 5
Spot Radius	(°)	—	14 ± 4	—	12 ± 5
Spot T-factor	(T_{spot} / T_{eff})	—	1.16 ± 0.05	—	1.17 ± 0.09
Spot 2 on Star 2			Cool Spot		Cool Spot
Colatitude	(°)	—	78 ± 4	—	—
Longitude	(°)	—	2 ± 1	—	—
Spot Radius	(°)	—	12 ± 4	—	—
Spot T-factor	(T_{spot} / T_{eff})	—	0.90 ± 0.05	—	—

strong correlations of the parameters and the Kurucz stellar atmosphere model was applied. The fixed inputs included standard convective parameters: gravity darkening, $g_1 = g_2 = 0.32$ (Lucy 1968), albedo value $A_1 = A_2 = 0.5$ (Ruciński 1969), and the effective temperature of the cooler star, T_2, was set to the value determined in section 3.2, 5471K. Logarithmic limb darkening coefficients were calculated by the WD program from tabulated values using the method of Van Hamme (1993). The solution's adjustable parameters include the inclination (i), mass ratio ($q = M_2 / M_1$), potential (Ω, $\Omega_1 = \Omega_2$), temperature of the primary star (T_1), and the normalized flux for each wavelength (L). The best-fit solutions for each data set are shown in Table 3 (columns 3 and 5). The fill-out parameter calculated was defined by Lucy and Wilson (1979) and is given by:

$$f = \frac{\Omega_{inner} - \Omega}{\Omega_{inner} - \Omega_{outer}} \quad (6)$$

where Ω_{inner} and Ω_{outer} are the inner and outer critical equipotential surfaces and Ω is the equipotential surface which describes the stellar surface. BM3 was used to calculate the fill-out values, which are reported in Table 3 for each solution. No third light was noted when included in the adjustable parameters. Only negligible small values resulted, indicating no appreciable contribution to the system's light. The normalized light curves for each passband overlaid by the synthetic solution curves (solid lines) are shown in Figure 5, with the residuals shown in Figure 6.

3.4. Spot model

The asymmetries in eclipsing binary light curves are usually attributed to large cool spots, hot regions such as faculae or gas streams that impact one of the stars. To fit the asymmetries in the light curves a second model was attempted for both DS1 and DS2. Excess light was noted in all five residual curves center at about phase 0.8 (see Figure 6). An over-luminous spot was added to both models to account for this excess light. A deficit of light was also noted between phase 0.2 and 0.5 in the three residual curves from S1. This required a second under-luminous spot in that model. BM3 was used again to obtain a good fit between the synthetic and observed light curves by adjusting each spot's parameters (latitude, longitude, spot size, and temperature). The best-fit spot parameter values from BM3

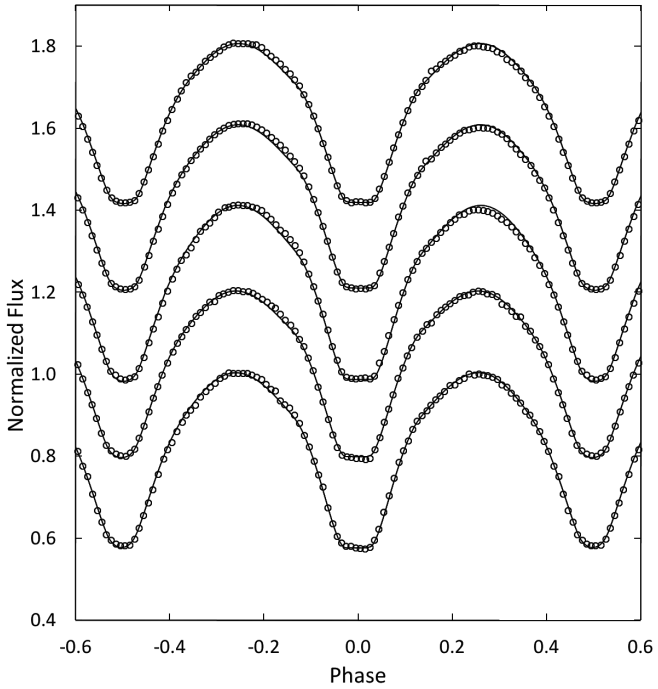

Figure 5. The WD model fit without spots (solid curve) to the observed normalized flux curves for each passband. From top to bottom the passbands are Sloan i', Sloan r', Sloan g', Johnson V, and Johnson B. The Sloan passbands are for solution S1 and the Johnson passbands are for solution S2. Each curve is offset by 0.2 for this combined plot. The best-fit parameters are given in columns 3 and 5 of Table 3. Error bars are omitted from the points for clarity.

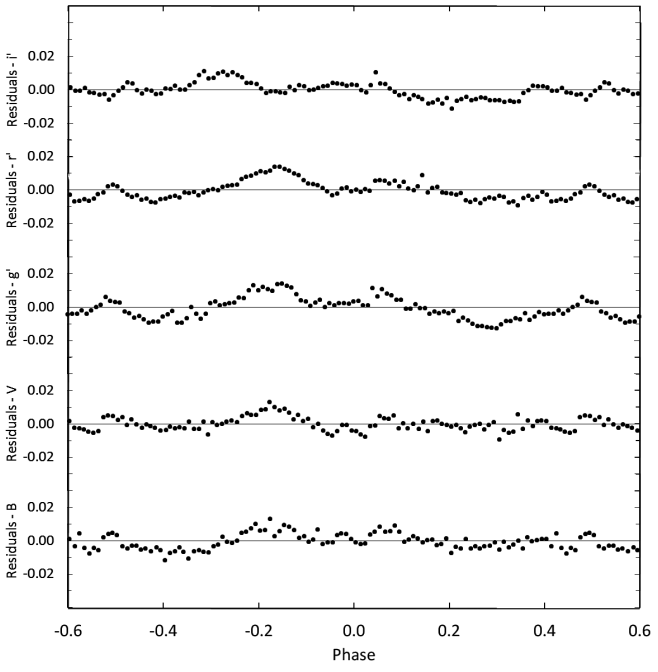

Figure 6. The residuals for the best-fit WD model without spots. The g', r', and i' residuals are from S1 and B and V from S2. Error bars are omitted from the points for clarity.

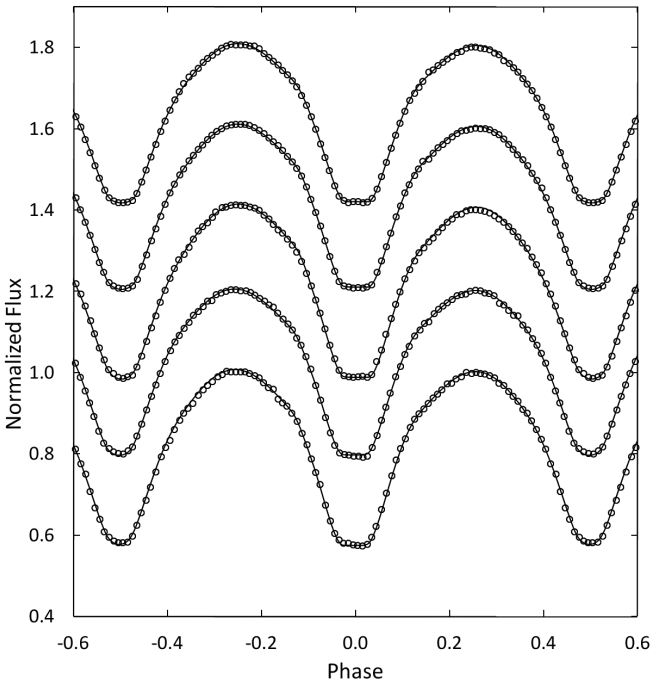

Figure 7. The WD model fit with spots (solid curve) to the observed normalized flux curves for each passband. From top to bottom the passbands are Sloan i', Sloan r', Sloan g', Johnson V, and Johnson B. The Sloan passbands are for solution S1 and the Johnson passbands are for solution S2. Each curve is offset by 0.2 for this combined plot. The best-fit parameters are given in columns 4 and 6 of Table 3. Error bars are omitted from the points for clarity.

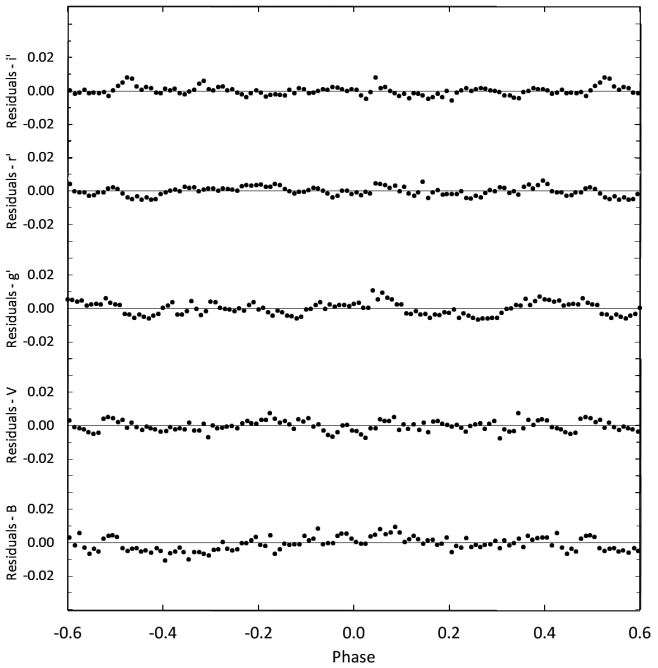

Figure 8. The bottom panel shows the residuals for the spotted WD model in each passband. The g', r', and i' residuals are from S1 and B and V from S2. Error bars are omitted from the points for clarity.

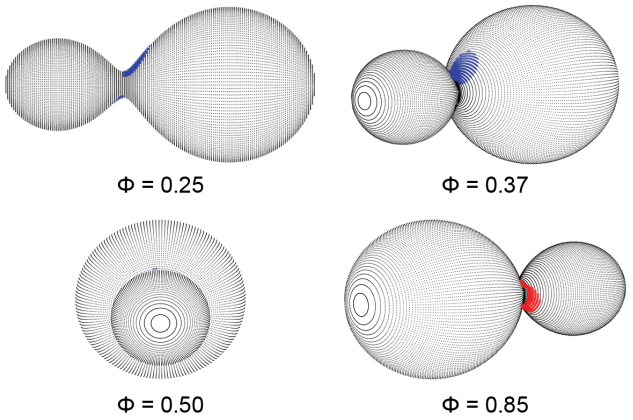

Figure 9. Roche Lobe surfaces of the best-fit WD spot model from S1 with orbital phase shown below each diagram.

Table 4. Provisional stellar parameters for V2790 Ori.

Parameter	*Symbol*	*Value*
Stellar masses	M_1 ($M_\odot$)	0.30
	M_2 ($M_\odot$)	0.96
Semi-major axis	a ($R_\odot$)	1.98
Stellar radii	R_1 ($R_\odot$)	0.58
	R_2 ($R_\odot$)	0.97
Surface gravity	log g_1 (cgs)	4.39
	log g_2 (cgs)	4.44
Mean density	$\overline{\rho}_1$ (g cm^{-3})	2.17
	$\overline{\rho}_2$ (g cm^{-3})	1.46
Stellar luminosity	L_1 V ($L_\odot$)	0.28
	L_2 V ($L_\odot$)	0.68
Bolometric magnitude	$M_{bol,1}$	6.05
	$M_{bol,2}$	5.05

Values in this table are provisional (calculated). Radial Velocity observations are necessary for direct determination of M_1, M_2, and a.

were then included in new WD solution attempts. The stellar parameters from the first solution were held fixed while the spot parameters were adjusted until the solution converged. The spot parameters were then held fixed and the stellar parameters adjusted until the solution converged again. This process was repeated until the model converged to a final solution. The final values for the spotted solution parameters are shown in columns 4 and 6 in Table 3. Figure 7 shows the spotted model fit (solid lines) to the observed light curve for each passband and solution. Figure 8 shows the residuals for the spotted models. For S1 the sum of the residuals squared was 0.0056 for the spotted model and 0.0196 for the unspotted model (3.5 times larger). For S2 the sum of the residuals squared was 0.0053 for the spotted model and 0.0082 for the unspotted model (1.5 times larger). A graphical representation of the spotted S1 solution is shown in Figure 9.

It is interesting to note that the resulting stellar parameters for the spotted S1 and S2 models agreed well except for the spot configuration. S2 did not require the under-luminous spot found in S1. The over-luminous (hot spot) modeled in S1 was found in S2 at almost the same location, size, and temperature. Since the two data sets were separated by 8 months this particular spot may be a long-lived feature in the primary star's photosphere while the under-luminous spot seems to have disappeared.

4. Discussion and conclusions

Several stellar parameters can now be determined. An estimate for the mass of the larger cooler star was found to have a value of $M_2 = 0.96 \pm 0.07\ M_\odot$ (see section 3.2). This value combined with the S1 mass ratio (q) gives a mass for the smaller hotter star of $M_1 = 0.30 \pm 0.07\ M_\odot$. Applying Kepler's Third Law gives the distance between the star's mass centers as $1.98 \pm 0.01\ R_\odot$. Mochnacki (1981) showed the mean stellar densities for contact binaries are given by:

$$\overline{\rho}_1 = \frac{0.0189}{r_1^3\,(1+q)\,P^2} \quad \text{and} \quad \overline{\rho}_2 = \frac{0.0189q}{r_2^3\,(1+q)\,P^2}\ , \qquad (7)$$

where the stellar radius is normalized to the semimajor axis and P is in days. The computed values are $\overline{\rho}_1 = 2.18$ g cm^{-3} and $\overline{\rho}_2 = 1.47$ g cm^{-3}. Additional stellar parameters were computed with the Wilson and Devinney (1971) light curve program (LC). All the computed stellar parameters are collected in Table 4.

The distance to V2790 Ori can be estimated using an empirical formula derived by Ruciński and Duerbeck (1997) which is given by:

$$M_v = -4.44 \log_{10} P + 3.02\,(B-V)_0 + 0.12. \qquad (8)$$

Equation 8 gives a distance modulus of $(m - M)_v = 4.76$ and distance of 183 ± 19 pc. An additional determination of distance can be made using the bolometric magnitudes in Table 4 combined with the bolometric corrections from Pecaut and Mamajek (2013). The correction for the primary star is $BC_{v1} = -0.14$ and $BC_{v2} = -0.18$ for the secondary star. The calculated magnitude for the system is $M_v = 4.87$, which gives a distance of 174 pc. The two distance determinations differ by about 5% but are a little closer than the 199 pc distance found by Gettel (2006).

W UMa-type binaries most often consist of two cool stars in contact whose spectral types are F, G, or K and their components have nearly equal surfaces temperatures in spite of their often greatly differing masses. This study confirms that V2790 Ori is a member of this class of eclipsing binaries with a high mass ratio of 3.15 and stars differing in temperature by only 150 K. It is a member of the W-type subclass where the larger more massive star is cooler and has less surface brightness than its companion and primary eclipse is an occultation. The best-fit WD solutions with fill-out values between 0.12 and 0.17 are consistent with a contact binary. No secular period change was found but this system needs to be monitored regularly for a possible third body in the system. A spectroscopic radial velocity study of this system, when combined with the photometric solution presented here, would be invaluable in determining the absolute properties of the stars.

5. Acknowledgements

The author wishes to thank Dr. Norman Markworth for reviewing this manuscript and his guidance in the use of the WD program. This research has made use of the SIMBAD database, operated at CDS, Strasbourg, France. This research was made possible through the use of the AAVSO Photometric All-Sky Survey (APASS), funded by the Robert Martin Ayers Sciences Fund.

References

Bradstreet, D. H., and Steelman, D. P. 2002, *Bull. Amer. Astron. Soc.*, **34**, 1224.
Diethelm, R. 2011, *Inf. Bull. Var. Stars*, No. 5960, 1.
Diethelm, R. 2012, *Inf. Bull. Var. Stars*, No. 6011, 1.
Gettel, S. J., Geske, M. T., and McKay, T. A. 2006, *Astron. J.*, **131**, 621.
Henden, A. A., *et al.* 2014, AAVSO Photometric All-Sky Survey, data release 9 (http:www.aavso.org/apass).
Hübscher, J. 2013, *Inf. Bull. Var. Stars*, No. 6084, 1.
Kafka, S. 2015, observations from the AAVSO International Database (https:/www.aavso.org/aavso-international-database).
Kwee, K. K., and van Woerden, H. 1956, *Bull. Astron. Inst. Netherlands*, **12**, 327.
Lucy, L. B. 1968, *Astrophys. J.*, **151**, 1123.
Lucy, L. B., and Wilson, R. E. 1979, *Astrophys. J.*, **231**, 502.
Mirametrics. 2015, Image Processing, Visualization, Data Analysis (http://www.mirametrics.com).
Mochnacki, S. W. 1981, *Astrophys. J.*, **245**, 650.
Nagai, K. 2012, *Var. Star Obs. League Japan*, No. 53, 1**.**
Nagai, K. 2013a, *Var. Star Obs. League Japan*, No. 55, 1.
Nagai, K. 2013b, *Var. Star Obs. League Japan*, No. 56, 1.
Nelson, R. H. 2011, *Inf. Bull. Var. Stars*, No. 5966, 1.
Nelson, R. H. 2012, *Inf. Bull. Var. Stars*, No. 6018, 1.
Otero, S. A., Wils, P., and Dubovsky, P. A. 2004, *Inf. Bull. Var. Stars*, No. 5570, 1.
Pecaut, M. J., and Mamajek, E. E. 2013, *Astrophys. J., Suppl. Ser.*, **208**, 9 (http://www.pas.rochester.edu/~emamajek/EEM_dwarf_UBVIJHK_colors_Teff.txt).
Qian, S. 2003, *Mon. Not. Roy. Astron. Soc.*, **342**, 1260.
Ruciński, S. M. 1969, *Acta Astron.*, **19**, 245.
Ruciński, S. M., and Duerbeck, H. W. 1997, *Publ. Astron. Soc. Pacific*, **109**, 1340.
Schlafly, E. F., *et al.* 2014, *Astrophys. J.*, **789**, 15 (http://faun.rc.fas.harvard.edu/eschlafly/2dmap/querymap.php).
Van Hamme, W. 1993, *Astron. J.*, **106**, 2096.
Van Hamme, W., and Wilson, R. E. 1998, *Bull. Amer. Astron. Soc.*, **30**, 1402.
Wang, J. M. 1994, *Astrophys. J.*, **434**, 277.
Wilson, R. E. 1990, *Astrophys. J.*, **356**, 613.
Wilson, R. E., and Biermann, P. 1976, *Astron. Astrophys.*, **48**, 349.
Wilson, R. E., and Devinney, E. J., 1971, *Astrophys. J.*, **166**, 605.
Wozniak, P. R., *et al.* 2004, *Astron. J.*, **127**, 2436.